Journal of Solid State Chemistry 182 (2009) 265–272

Contents lists available at ScienceDirect

Journal of Solid State Chemistry

journal homepage: www.elsevier.com/locate/jssc

Structure and magnetic properties of RE_2Cu_2Cd

Falko M. Schappacher, Wilfried Hermes, Rainer Pöttgen *

Institut für Anorganische und Analytische Chemie, Universität Münster, Corrensstrasse 30, D-48149 Münster, Germany

ARTICLE INFO

Article history:
Received 8 September 2008
Received in revised form
22 October 2008
Accepted 25 October 2008
Available online 12 November 2008

Keywords:
Intermetallic compounds
Crystal chemistry
RE_2Cu_2Cd
Magnetic materials

ABSTRACT

The ternary intermetallic compounds RE_2Cu_2Cd (RE = Y, Sm, Gd–Tm, Lu) were synthesized by induction-melting of the elements in sealed tantalum tubes. The samples were characterized by X-ray powder diffraction. The structure of Gd_2Cu_2Cd was refined from single crystal X-ray diffractometer data: Mo_2FeB_2 type, space group $P4/mbm$, $a = 756.2(3)$, $c = 380.2(3)$ pm, w$R2 = 0.0455$, 321 F^2 values, 12 variables. The structures are 1:1 intergrowth variants of slightly distorted CsCl and AlB_2 related slabs of compositions RECd and $RECu_2$. The copper and cadmium atoms build up two-dimensional [Cu_2Cd] networks (257 pm Cu–Cu and 301 pm Cu–Cd in Gd_2Cu_2Cd) which are bonded to the rare earth atoms via short RE–Cu contacts (290 pm in Gd_2Cu_2Cd). Temperature dependent susceptibility measurements of RE_2Cu_2Cd with RE = Gd, Tb, Dy, and Tm show experimental magnetic moments which are close to the free RE^{3+} ion values. The four compounds show ferromagnetic ordering at $T_C = 116.7(2)$, 86.2(3), 48.4(1), and 14.5(1) K, respectively, as confirmed by heat capacity measurements. Dy_2Cu_2Cd shows a spin reorientation at $T_N = 16.9(1)$ K.

1. Introduction

The intermetallic compounds RE_2T_2X (RE = rare earth metal, T = transition metal and X = In, Sn, Mg, Cd) with Mo_2B_2Fe [1] and Er_2Au_2Sn [2] (U_2Pt_2Sn [3]) type structure have been extensively studied in the last 15 years for their interesting physical properties. An overview is given in a recent review article [4]. The indides and stannides of these series have intensively been investigated, while only little information is available for the corresponding magnesium and cadmium compounds. The compounds containing indium or tin are synthesized via arc-melting without significant risks of evaporations. Due to the comparatively low boiling points of magnesium (1363 K) and cadmium (1038 K) [5] preparation in a quasi-open setup would result in significant weight losses through evaporation. Consequently the RE_2T_2Mg and RE_2T_2Cd compounds need to be synthesized in sealed tantalum or niobium ampoules [6].

With cadmium, the series of RE_2Ni_2Cd (RE = La, Ce, Pr, Nd, Sm, Tb, Dy) [7,8], RE_2Rh_2Cd (RE = La, Ce, Pr, Nd, Sm) [9], RE_2Pd_2Cd (RE = La, Ce, Nd) [6,10], Ce_2Pt_2Cd [6] and RE_2Au_2Cd (RE = La, Ce, Pr, Nd, Sm, Gd) [11–13] compounds have been synthesized. The cell volumes of $Ce_2Ni_{1.88}Cd$ and $Ce_2Rh_{1.86}Cd$ strongly deviate from the Iandelli plots. Both compounds show intermediate-valent cerium [7,9]. Ce_2Au_2Cd contains stable trivalent cerium and can be considered as a heavy fermion system with antiferromagnetic ordering around 5 K [12]. Gd_2Au_2Cd exhibits ferromagnetism and spin-glass anomalies [13].

Recently we reported on the magnetic and heat capacity data of RE_2Pd_2Cd (RE = La, Ce, Nd) [10]. In this series La_2Pd_2Cd is a Pauli-paramagnet, Ce_2Pd_2Cd an antiferromagnet with Kondo interactions and Nd_2Pd_2Cd orders ferromagnetically at $T_C = 23.7$ K. Later on also the structural data and physical properties of the series RE_2Pd_2Cd (RE = Pr, Sm, Gd–Lu) have been investigated [14]. In continuation of our investigations on RE_2T_2Cd intermetallics, here we present the structure, magnetic and heat capacity data of RE_2Cu_2Cd for RE = Y, Sm, Gd–Tm, Lu.

2. Experimental

2.1. Synthesis

The starting materials for the preparation of the RE_2Cu_2Cd samples were ingots of the rare earth elements (Johnson-Matthey, Kelpin, or smart elements), copper shot (Johnson-Matthey) and a cadmium rod (Johnson-Matthey), all with a stated purity better than 99.9 at.% (metal content). The rare earth ingots were cut into smaller pieces and arc-melted [15] into small buttons under an argon atmosphere of approximately 600 mbar. The argon was purified with molecular sieves, silica gel, and titanium sponge (900 K). The pre-melting procedure reduces shattering during the exothermic reaction with copper and cadmium. The elements were weighed in the ideal 2:2:1 atomic ratio and sealed in tantalum tubes under argon. The ampoules were then placed in a

* Corresponding author. Fax: +49 251 83 36002.
E-mail address: pottgen@uni-muenster.de (R. Pöttgen).

0022-4596/$ - see front matter © 2008 Elsevier Inc. All rights reserved.
doi:10.1016/j.jssc.2008.10.033

water cooled quartz sample chamber of an induction furnace (Hüttinger Elektronik, Freiburg, type TIG 1.5/300) under flowing argon [16] and first heated to ca. 1420 K (for $RE = Sm$), respectively ca. 1470 K ($RE = Y$, Gd–Lu), for about 5 min followed by annealing at 1070 K for 3–5 h. The temperature was controlled by a Sensor Therm Methis MS09 pyrometer with an accuracy of ±30 K.

2.2. EDX analyses

The phase purity of the bulk samples and of the Gd_2Cu_2Cd single crystal investigated on the diffractometer was analyzed using a Leica 420I scanning electron microscope. The rare earth trifluorides, copper and cadmium were used as standards. No impurity elements heavier than sodium were observed. The experimentally determined compositions were very close to the ideal ones. The semiquantitative EDX analysis gave no hint for homogeneity ranges.

Table 1
Lattice parameters of the tetragonal intermetallic compounds RE_2Cu_2Cd.

Compound	a (pm)	c (pm)	V (nm^3)
Y_2Cu_2Cd	750.4 (1)	375.0 (1)	0.2112
Sm_2Cu_2Cd	760.2 (1)	381.8 (1)	0.2206
Gd_2Cu_2Cd	756.2 (3)	380.2 (3)	0.2174
Tb_2Cu_2Cd	754.6 (2)	377.2 (1)	0.2148
Dy_2Cu_2Cd	749.0 (2)	374.2 (2)	0.2100
Ho_2Cu_2Cd	747.9 (2)	372.4 (1)	0.2083
Er_2Cu_2Cd	746.2 (2)	370.5 (2)	0.2063
Tm_2Cu_2Cd	743.9 (2)	368.7 (2)	0.2040
Lu_2Cu_2Cd	738.9 (1)	365.3 (1)	0.1994

Table 2
Crystal data and structure refinement for Gd_2Cu_2Cd.

Empirical formula	Gd_2Cu_2Cd
Molar mass	553.98 g mol^{-1}
Radiation	Ag$K\alpha$ ($\lambda = 56.083$ pm)
Crystal system	tetragonal
Space group	$P4/mbm$ (No. 127)
Pearson symbol	$tP10$
Unit cell dimensions	$a = 756.2(3)$ pm
(Guinier powder data)	$c = 380.2(3)$ pm
	$V = 0.2174$ nm^3
Formula units per cell	$Z = 2$
Calculated density	8.46 g cm^{-3}
Crystal size	$10 \times 40 \times 90$ μm^3
Transmission (max/min)	0.973/0.524
Absorption coefficient	23.5 mm^{-1}
$F(000)$	468
θ range for data collection	3–30°
Range in $h\,k\,l$	±12, ±12, +6
Total no. reflections	2222
Independent reflections	321 ($R_{int} = 0.0692$)
Reflections with $I > 2\sigma(I)$	288 ($R_\sigma = 0.0289$)
Data/parameters	321/12
Goodnes-of-fit on F^2	1.081
Final R indices [$I > 2\sigma(I)$]	$R1 = 0.0209$
	w$R2 = 0.0440$
R indices (all data)	$R1 = 0.0270$
	w$R2 = 0.0455$
Extinction coefficient	0.0040(8)
Largest diff. peak and hole	1.45/−3.01 eÅ^{-3}

Table 3
Atomic coordinates and anisotropic displacement parameters (pm^2) of Gd_2Cu_2Cd.

Atom	*Wyck.*	x	y	z	$U_{11} = U_{22}$	U_{33}	U_{12}	U_{eq}
Gd	4*h*	0.17556 (3)	1/2+x	1/2	116 (1)	102 (2)	−14 (1)	112 (1)
Cu	4*g*	0.38006 (9)	1/2+x	0	123 (3)	130 (3)	−29 (3)	125 (2)
Cd	2*a*	0	0	0	113 (2)	176 (3)	0	134 (2)

U_{eq} is defined as one third of the trace of the orthogonalized U_{ij} tensor.

Table 4
Interatomic distances (pm) of Gd_2Cu_2Cd calculated with the lattice parameters obtained from X-ray powder data.

Gd:	2	Cu	289.8	Cu:	1	Cu	256.5
	4	Cu	296.4		2	Gd	289.8
	4	Cd	337.6		4	Gd	296.4
	1	Gd	375.5		2	Cd	301.4
	2	Gd	380.2	Cd:	4	Cu	301.4
	4	Gd	394.5		8	Gd	337.6

Standard deviations are equal or less than 0.2 pm. All distances within the first coordination spheres are listed.

Table 5
Magnetic data of the RE_2Cu_2Cd compounds.

Compound	μ_{exp} (μ_B/*RE* atom)	Θ (K)	T_C (K)	μ_{sm} (μ_B/*RE* atom)
Gd_2Cu_2Cd	7.79 (1)	109.9 (1)	117 (1)	6.2 (1)
Tb_2Cu_2Cd	9.89 (1)	45.1 (3)	87 (1)	5.34 (2)
Dy_2Cu_2Cd	10.89 (1)	54.0 (3)	48.3 (2)	8.60 (1)
Tm_2Cu_2Cd	7.70 (1)	25.3 (3)	16.6 (2)	6.7 (1)

μ_{exp}: experimental magnetic moment in the paramagnetic range; Θ: paramagnetic Curie temperature; T_C: Curie temperature; μ_{sm}: saturation magnetization at 5 K and 80 kOe.

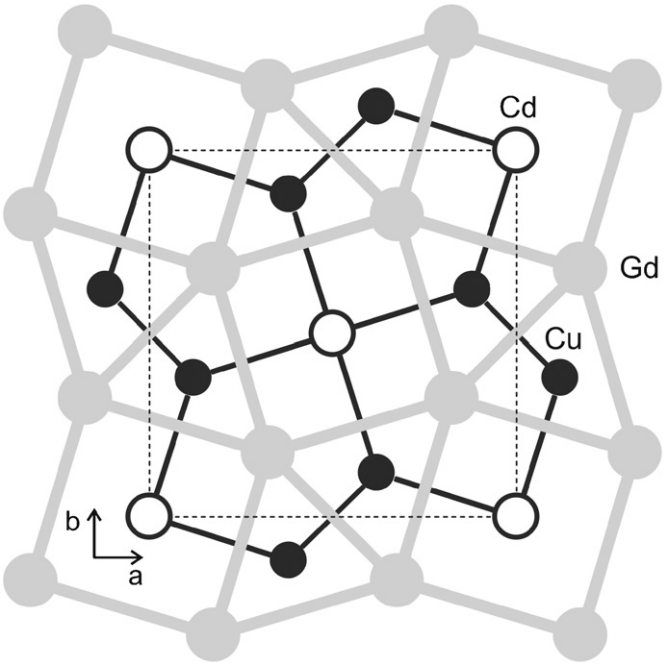

Fig. 1. Projection of the Gd_2Cu_2Cd structure onto the *ab* plane. All atoms lie on mirror planes at $z = 0$ (thin lines) and $z = 1/2$ (thick lines). Gadolinium, copper and cadmium atoms are drawn as medium gray, black, and open circles, respectively.

2.3. X-ray image plate data and data collection

The samples were analyzed by powder X-ray diffraction on a Guinier camera (equipped with an image plate system Fujifilm, BAS-1800) using Cu$K\alpha_1$ radiation and α-quartz ($a = 491.30$, $c = 540.46$ pm) as an internal standard. The tetragonal lattice parameters (Table 1) were obtained from least-squares refinements of the powder data. The correct indexing of the diffraction lines was ensured by intensity calculations [17] using the positional parameters of Gd_2Cu_2Cd obtained during the present investigation.

Irregularly shaped smaller crystal fragments of Gd_2Cu_2Cd were obtained from the larger lump by mechanical fragmentation. They were glued to quartz fibres usings bees wax and were first investigated by Laue photographs on a Buerger camera (white molybdenum radiation, image plate technique, Fujifilm, BAS-1800) in order to check the quality for intensity data collection. Intensity data were collected at room temperature by use of an Enraf-Nonius CAD4 diffractometer with graphite monochromatized Ag$K\alpha$ radiation ($\lambda = 56.083$ pm) and a scintillation counter with pulse height discrimination. Scans were taken in the $\omega/2\theta$ mode. ψ-Scan data were used for an empirical absorption correction followed by a spherical absorption correction. All relevant crystallographic data and details of the data collection and evaluation are listed in Table 2.

2.4. Physical property measurements

Heat capacity and magnetic measurements were performed on polycrystalline samples using a quantum design physical property measurement system. The samples were glued to a pre-calibrated heat capacity puck using *Apiezon N* grease which also provides good thermal contact between the sample and the platform. The transition temperatures for all compounds were determined from the inflection points of the lambda-type anomalies. For magnetic susceptibility measurements (all data refer to $\chi = M/H$ throughout the manuscript) the samples were packed in kapton foil and attached to the sample holder rod of a VSM. The transition temperatures (Table 5) of the magnetic data were determined from the derivatives of the field-cooling measurements (*vide infra*).

3. Results and discussion

3.1. Structure refinement

The diffractometer data set of Gd_2Cu_2Cd showed a primitive tetragonal cell and the systematic extinctions were compatible with the space group $P4/mbm$, similar to the RE_2Pd_2Cd series [10,14]. The Mo_2B_2Fe structure type for Gd_2Cu_2Cd was already

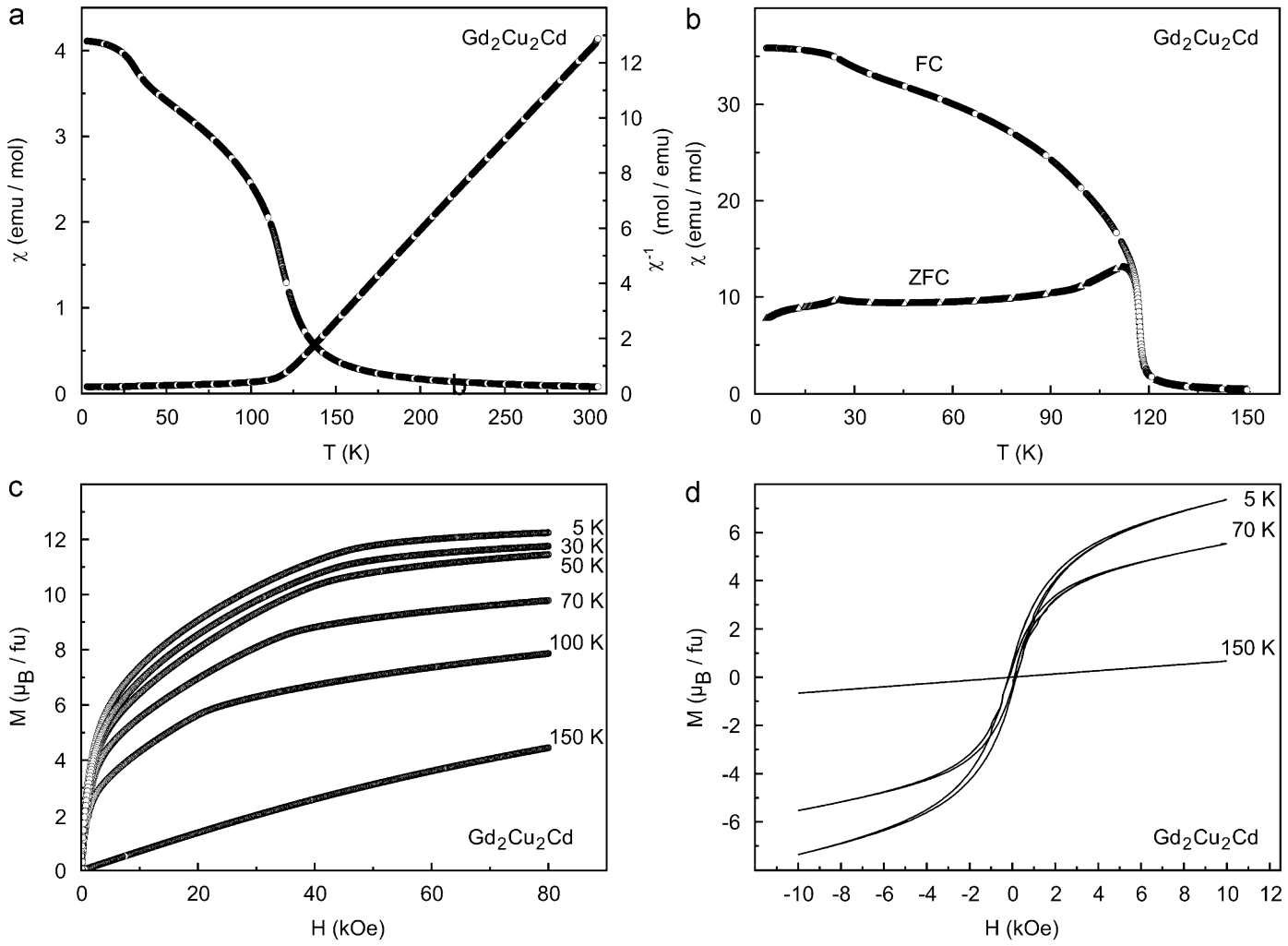

Fig. 2. (a) Susceptibility χ and inverse susceptibility χ^{-1} for Gd_2Cu_2Cd in $H = 10$ kOe. (b) Low field ($H = 100$ Oe) susceptibility measured in ZFC and FC states of the sample. (c) High field magnetization at $T = 5$, 30, 50, 70, 100 and 150 K. (d) Hysteresis loops measured at $T = 5$, 70 and 150 K.

evident from the Guinier powder data. The atomic parameters of Gd_2Pd_2Cd [14] were taken as starting parameters and the structure was refined using Shelxl-97 [18] (full-matrix least-squares on F^2) with anisotropic atomic displacement parameters for all atoms. As a check for the correct composition, the occupancy parameters were refined in a separate series of least-squares cycles. For Gd_2Cu_2Cd all sites were fully occupied within two standard uncertainties and in the final cycles the ideal occupancies were assumed again. The positional parameters and interatomic distances are listed in Tables 3 and 4. Further details on the structure refinement are available from Fachinformationszentrum Karlsruhe, D-76344 Eggenstein-Leopoldshafen (Germany), by quoting the Registry No. CSD-419851 (Table 5).

3.2. Crystal chemistry

The new RE_2Cu_2Cd (RE = Y, Sm, Gd–Lu) compounds crystallize with the tetragonal Mo_2B_2Fe structure [1], space group $P4/mbm$, a ternary ordered variant of the U_3Si_2 type [19,20]. In Fig. 1 we present a projection of the Gd_2Cu_2Cd structure onto the ab plane. From a geometrical point of view, the structure consists of two different layers with gadolinium atoms at $z = 1/2$ and a two-dimensional [Cu_2Cd] network at $z = 0$. The gadolinium atoms form square prisms around the cadmium and trigonal prisms around the copper atoms. The structure can therefore be considered as a 1:1 intergrowth of AlB_2 and CsCl related slabs [4] of compositions $GdCu_2$ and GdCd.

Within the [Cu_2Cd] network the Cu–Cu distances of 257 pm are close to the Cu–Cu distance of 256 pm in *fcc* copper [21]. The Cu–Cd distances of 301 pm are significantly longer than the sum of the covalent radii of 258 pm [5], indicating only weak Cu–Cd interactions. The [Cu_2Cd] network is connected to the gadolinium layer via shorter Gd–Cu contacts (290–296 pm Gd–Cu). The Gd–Cu distances are slightly longer than the sum of the covalent radii of 278 pm [5]. These interactions strongly contribute to the stability of the compound.

The bonding patterns in the RE_2T_2X compounds can, to a first approximation, be derived from the course of the cell parameters. The a parameter (and consequently also the b parameter) are influenced by the T–X bonding, while the c parameter mostly depends on the size of the rare earth element. These bonding peculiarities have been described in detail for the two series RE_2Ni_2In vs. RE_2Ni_2Mg [22] and RE_2Cu_2In vs. RE_2Cu_2Mg [23]. In both cases, the indides have the smaller a parameters and electronic structure calculations revealed stronger Ni–In and Cu–In bonding as compared to Ni–Mg and Cu–Mg. Keeping these findings in mind, comparison of the lattice parameters of Gd_2Cu_2Mg ($a = 765.31$, $c = 377.22$ pm [23]) and Gd_2Cu_2Cd ($a = 756.2$, $c = 380.2$ pm) is indicative for stronger Cu–Cd bonding as compared to Cu–Mg. For further crystal chemical details we refer to a review article [4].

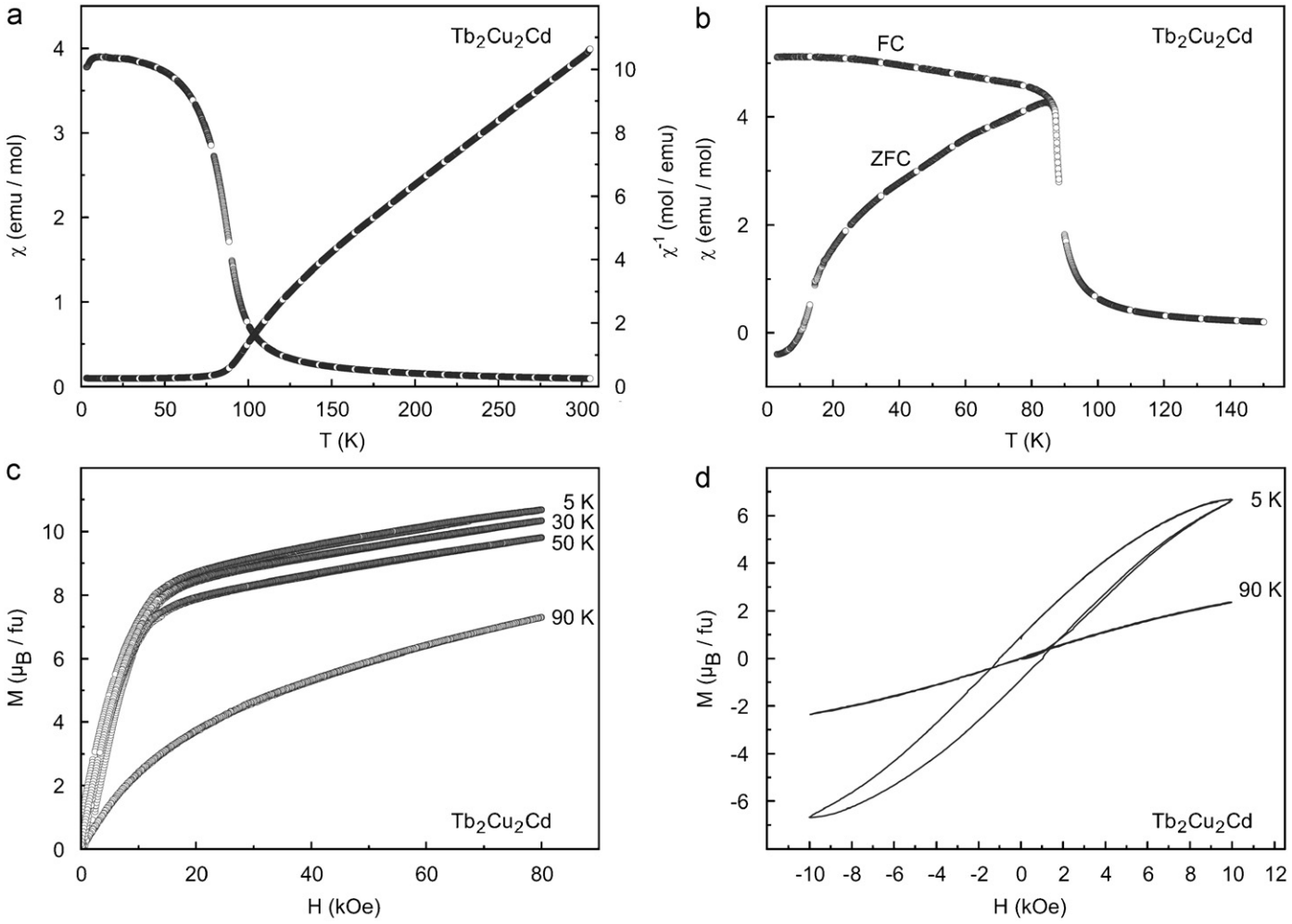

Fig. 3. (a) Susceptibility χ and inverse susceptibility χ^{-1} for Tb_2Cu_2Cd in $H = 10$ kOe. (b) Low field ($H = 100$ Oe) susceptibility measured in ZFC and FC states of the sample. (c) High field magnetization at $T = 5$, 30, 50 and 90 K. (d) Hysteresis loops measured at $T = 5$ and 90 K.

3.3. Magnetic properties

3.3.1. Gd_2Cu_2Cd

The magnetic data of Gd_2Cu_2Cd are plotted in Figs. 2a–d. The magnetic susceptibility ($\chi = M/H$) shown in Fig. 2a has been measured in a field of 10 kOe. Below 120 K an upturn of the susceptibility can be observed indicating ferromagnetic ordering. The inverse susceptibility χ^{-1} follows the Curie–Weiss law in the temperature range 150–305 K. The paramagnetic Curie temperature, $\Theta_P = 109.9(1)$ K, and the effective Bohr magneton number, $\mu_{eff} = 7.79(1)\,\mu_B$/Gd atom were calculated from the linear region of the plot of χ^{-1} vs. T in the range of 150–305 K. The observed value of μ_{eff} is close to the expected value for a free Gd^{3+} ion ($\mu_{eff} = 7.94\,\mu_B$). The positive value of Θ_P indicates ferromagnetic interactions. The anomaly around 30 K might be indicative for spin reorientations.

The low field susceptibility ($H = 100$ Oe) measured in zero field cooled (ZFC) and field cooled (FC) states of the sample is shown in Fig. 2b. The ZFC curve exhibits a sharp decrease at 117(1) K indicating the onset of the ferromagnetic ordering (T_C). In the FC measurement the moment value increases as T approaches 117 K and shows another upturn at around 27 K, which could be a hint for a further spin reordering. The hint for further ordering around 27 K needs to be investigated by more sensitive *ac* susceptibility measurements in the future.

The magnetization (M) as a function of the external field (H) at 5 K is consistent with the observation of the ferromagnetic ordering. M increases sharply for small changes in H, to higher fields the inclination of M becomes smaller and from 50 to 80 kOe M increases marginally. The saturation moment value at 5 K and 80 kOe is about $6.2(1)\,\mu_B$/Gd atom, which is slightly smaller than the expected value of $7\,\mu_B$/Gd atom for a full parallel spin alignment. The course of the isotherm at 5 K is typical for a so called canted ferromagnet. The observed hysteresis is very small.

3.3.2. Tb_2Cu_2Cd

In Figs. 3a–d we present the magnetic data of Tb_2Cu_2Cd. The susceptibility at an external field of 10 kOe in the range from 3 to 305 K is shown in Fig. 3a. Tb_2Cu_2Cd undergoes a paramagnetic to ferromagnetic transition at around 90 K, which can be seen as a sudden upturn in the plot of χ vs. T. The inverse susceptibility follows the Curie–Weiss law in the range of 150–305 K, leading to a paramagnetic Curie temperature, $\Theta_P = 45.1(3)$ K and an effective Bohr magneton number, $\mu_{eff} = 9.89(1)\,\mu_B$/Tb atom. The latter is close to the expected value for a free Tb^{3+} ion ($\mu_{eff} = 9.72\,\mu_B$). The positive Weiss constant indicates ferromagnetic interactions. The anomaly at low temperatures (Fig. 3a) might be indicative for spin reorientations. χ^{-1} deviates from Curie–Weiss behavior below 150 K.

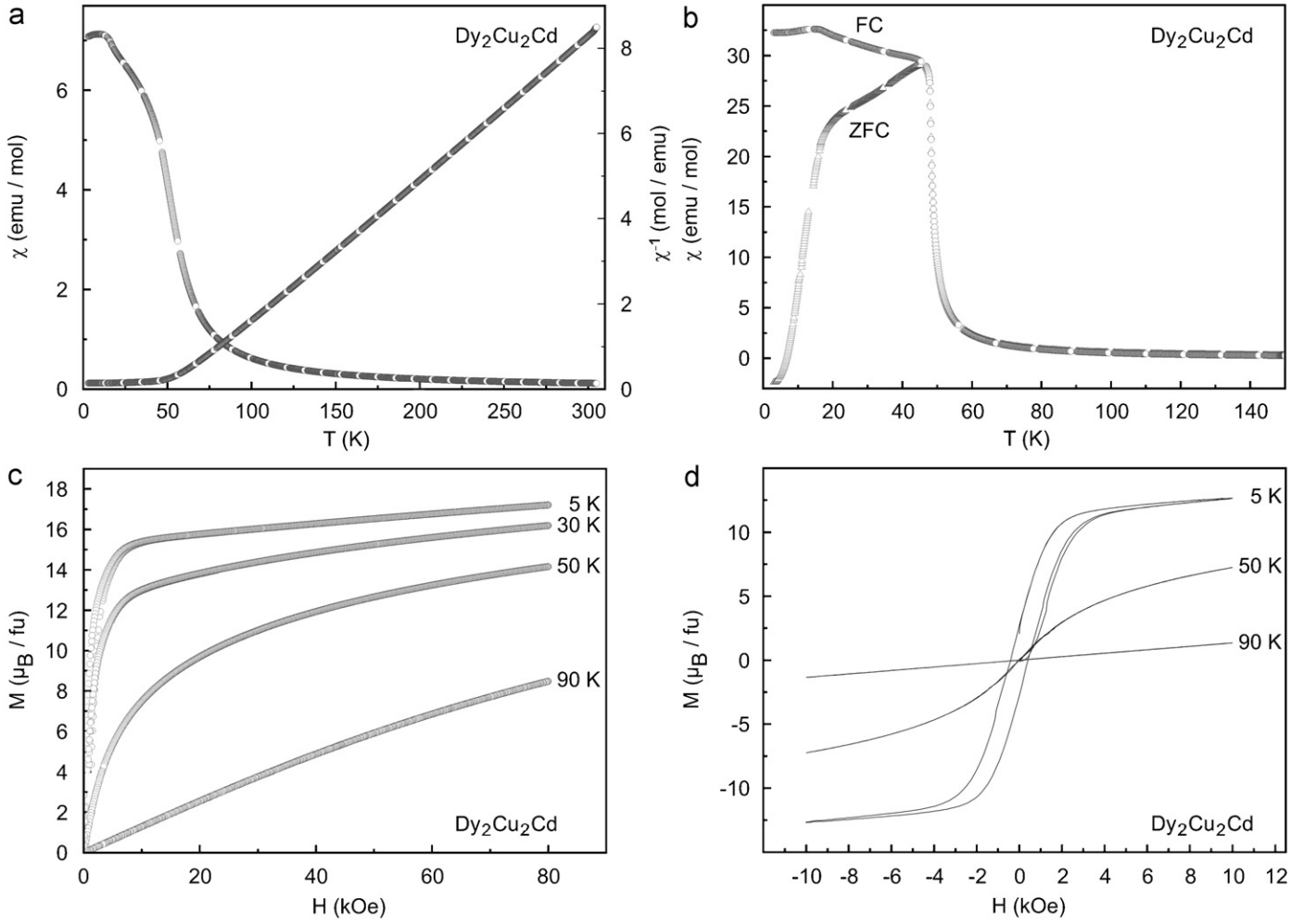

Fig. 4. (a) Susceptibility χ and inverse susceptibility χ^{-1} for Dy_2Cu_2Cd in $H = 10$ kOe. (b) Low field ($H = 100$ Oe) susceptibility measured in ZFC and FC states of the sample. (c) High field magnetization at $T = 5$, 30, 50 and 90 K. (d) Hysteresis loops measured at $T = 5$, 50 and 90 K.

The ZFC–FC behavior ($H = 100$ Oe) is shown in Fig. 3b. The FC curve shows a sharp upturn of the susceptibility at 87 K indicating the onset of ferromagnetic ordering. Down to 90 K the FC curve is parallel to the course of the ZFC curve.

The magnetization data between 5 and 90 K against the applied field H are plotted in Fig. 3c. The magnetization isotherms below T_C do not show such a strong dependency of M for small changes of H like Dy_2Cu_2Cd does (*vide infra*). This is the typical behavior for a ferromagnet. The saturation moment value at 5 K and 80 kOe is about 5.34(2) μ_B/Tb atom, which is less than the expected value of 9 μ_B/Tb atom.

Hysteresis loops have been recorded in the $\pm$10 kOe range (Fig. 3d). The 5 K isotherm shows a clear but small hysteresis and only a small coercive field.

In Fig. 4b the ZFC–FC susceptibility curves in a field of $H = 100$ Oe are plotted. The FC curve shows a sharp upturn around 48 K indicating ferromagnetic ordering and increases marginally up to 16 K. At around 16 K the curve shows a kink with decreasing susceptibility to lower temperatures indicating reorientation to an antiparallel spin alignment. From the derivative $d\chi/dT$ one can deduce the ordering temperatures $T_C = 48.3(2)$ K and $T = 16.1(5)$ K at which a spin reorientation takes place.

The magnetization data at different temperatures are shown in Fig. 4c. M increases sharply for small changes in H, and then increases marginally up to 80 kOe. The saturation moment value at 5 K and 80 kOe is about 8.60(1) μ_B/Dy atom, slightly smaller than the expected value of 10 μ_B/Dy atom. At 5 K a clear but small hysteresis is observed (Fig. 4d).

3.3.3. Dy_2Cu_2Cd

The magnetic data of Dy_2Cu_2Cd are plotted in Figs. 4a–d. The susceptibility in an external field of $H = 10$ kOe (Fig. 4a) shows a sharp upturn around 50 K, indicating magnetic ordering. Around 15 K there is a kink indicating a spin reorientation. The values of Θ_P and μ_{eff} are 54.0(3) K and 10.89(1) μ_B/Dy atom, respectively, which compares well with the theoretical value of 10.65 μ_B/Dy atom. The positive value of the paramagnetic Curie temperature indicates ferromagnetic interactions. The ZFC–FC behavior clearly establishes ferromagnetic ordering at $T_C = 48.3(2)$ K.

3.3.4. Tm_2Cu_2Cd

Susceptibility measurements of Tm_2Cu_2Cd have been performed in a field of 10 kOe in the temperature range 3–305 K. The data of χ and χ^{-1} are plotted in Fig. 5a. The susceptibility shows a sharp upturn around 20 K indicating magnetic ordering. From the Curie–Weiss behavior in the 150–305 K range one can deduce the values of Θ_P and μ_{eff} of 25.3(3) K and 7.70(1) μ_B/Tm atom, respectively. The experimental value compares well with the theoretical value of 7.56 μ_B for the free Tm^{3+} ion. The positive value of Θ_P indicates ferromagnetic interactions.

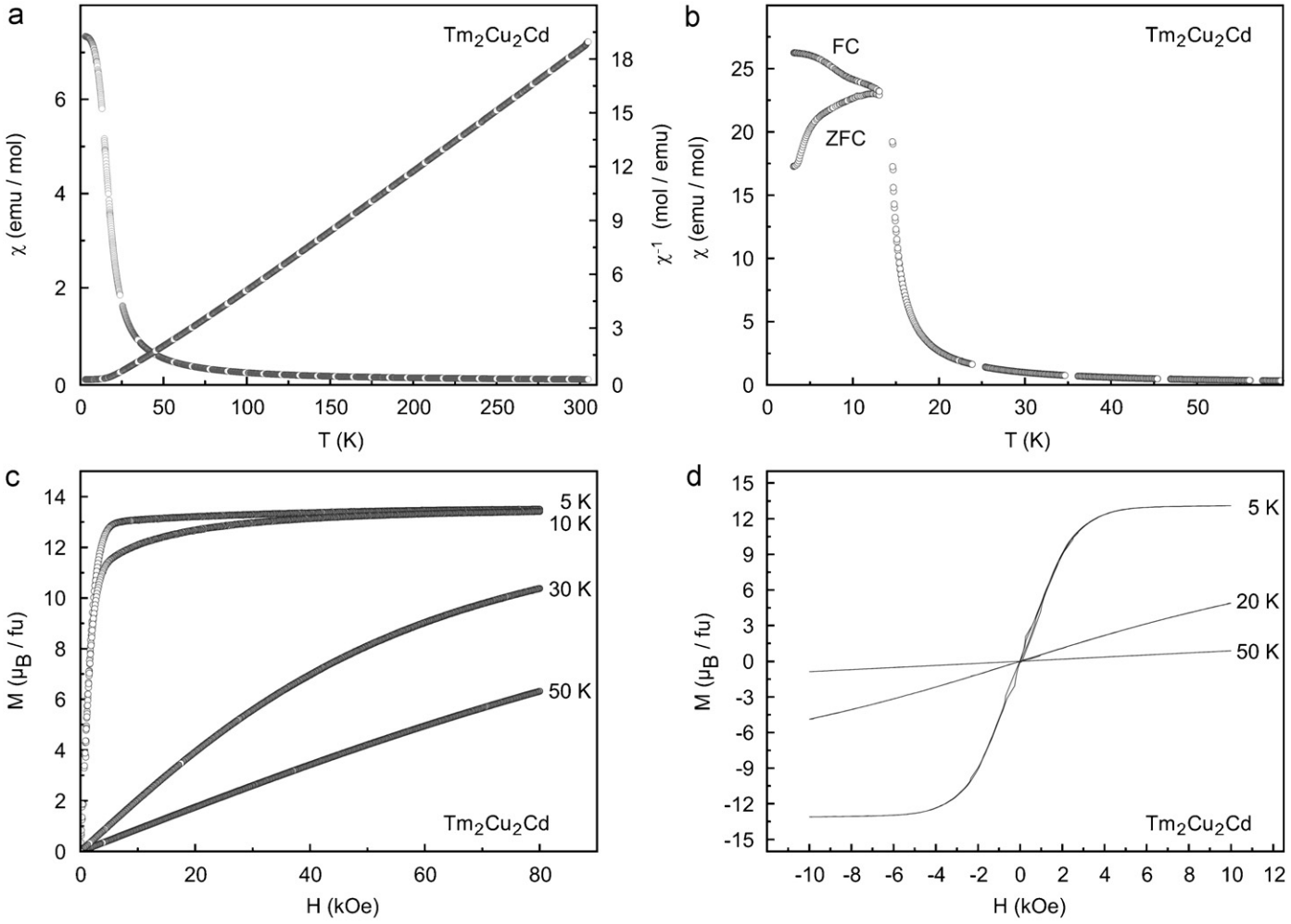

Fig. 5. (a) Susceptibility χ and inverse susceptibility χ^{-1} for Tm_2Cu_2Cd in $H = 10$ kOe. (b) Low field ($H = 100$ Oe) susceptibility measured in ZFC and FC states of the sample. (c) High field magnetization at $T = 5$, 10, 30 and 50 K. (d) Hysteresis loops measured at $T = 5$, 20 and 50 K.

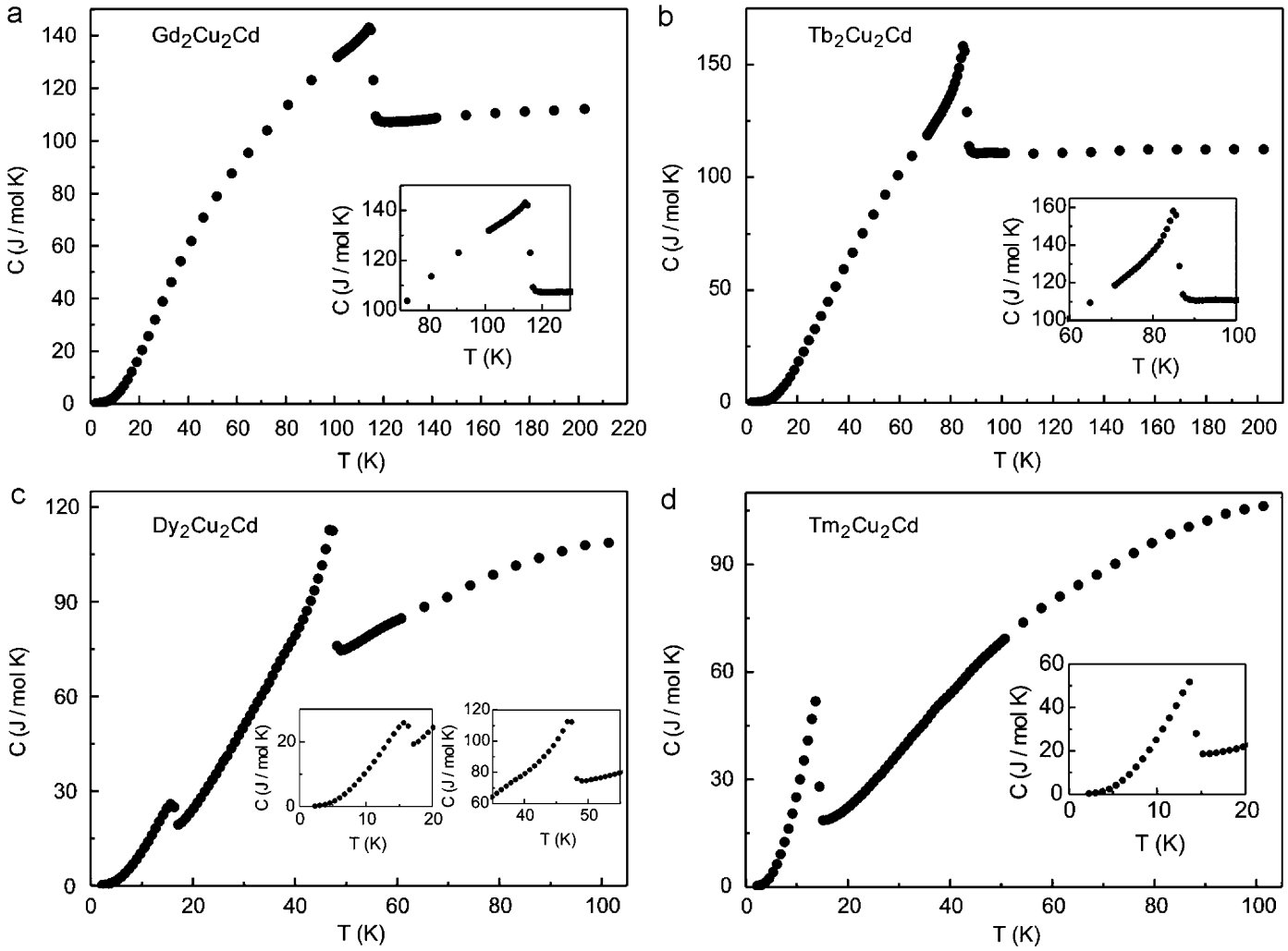

Fig. 6. Total heat capacity (C) as a function of temperature (T) for some RE_2Cu_2Cd compounds. The insets show an up-scale around the ordering temperatures.

The ZFC–FC susceptibility data in an external field of $H = 100$ Oe are plotted in Fig. 5b. The FC curve shows a sharp upturn around 15 K indicating ferromagnetic ordering. The precise ordering temperature of $T_C = 16.6(2)$ K was deduced from the derivative $d\chi/dT$.

The magnetization isotherms are shown in Fig. 5c. The 5 K isotherm shows typical behavior of a ferromagnet. M increases sharply for small changes in H and then saturates for higher H. At 5 K and a field of 80 kOe the value of the saturation moment is 6.7(1) μ_B/Tm, close to the theoretical value of 7 μ_B/Tm atom. At 5 K we observe a noteworthy hysteresis (Fig. 5d).

3.4. Heat capacity data

The heat capacity data for RE_2Cu_2Cd (RE = Gd, Tb, Dy, Tm) are plotted in Figs. 5a–d. The insets show an up-scale around the ordering temperatures. All measurements have been performed without an external field. The specific heat of Gd_2Cu_2Cd is shown in Fig. 5a. Up to the ordering temperature of $T_C = 116.7(2)$ K the heat capacity increases and then drops sharply. The heat capacity of Tb_2Cu_2Cd shows a similar behavior and a lambda-like transition (Fig. 5b) with an ordering temperature of $T_C = 86.2(3)$ K. The specific heat of Dy_2Cu_2Cd (Fig. 5c) shows two lambda-like transitions, which were already evident from the ZFC–FC susceptibility plot (Fig. 4b). The ordering temperatures are $T_C = 48.4(1)$ K and $T = 16.9(1)$ K. Similar behavior has been observed for Dy_2Cu_2In, which shows ferromagnetic ordering at $T_C = 45.5$ K and antiferromagnetic ordering at $T_N = 22.0$ K [24]. Tm_2Cu_2Cd (Fig. 5d) shows the lowest ordering temperature of the investigated compounds. The specific heat exhibits a lambda-like transition and the ordering temperature can be determined as $T_C = 14.5(1)$ K (Fig. 6).

4. Conclusions

The series of isostructural RE_2Cu_2Cd compounds with RE = Y, Sm, Gd–Tm, Lu was synthesized and structurally characterized. They crystallize with the Mo_2B_2Fe type, a ternary ordered version of the U_3Si_2 structure. Detailed investigations on the magnetic properties of Gd_2Cu_2Cd, Tb_2Cu_2Cd, Dy_2Cu_2Cd and Tm_2Cu_2Cd have been carried out. These four compounds show ferromagnetic ordering at low temperatures. Dy_2Cu_2Cd undergoes ferromagnetic ordering at $T_C = 48.4(1)$ K and antiferromagnetic ordering at $T_N = 16.9(1)$ K.

Acknowledgments

We are grateful to B. Heying for the intensity data collection. This work was supported by the Deutsche Forschungsgemeinschaft.

References

[1] W. Rieger, H. Nowotny, H. Benesovsky, Monatsh. Chem. 95 (1964) 1502.
[2] R. Pöttgen, Z. Naturforsch. 49b (1994) 1309.
[3] P. Gravereau, F. Mirambet, B. Chevalier, F. Weill, L. Fournès, D. Laffargue, F. Bourée, J. Etourneau, J. Mater. Chem. 4 (1994) 1893.
[4] M. Lukachuk, R. Pöttgen, Z. Kristallogr. 218 (2003) 767.
[5] J. Emsley, The Elements, Oxford University Press, Oxford, UK, 1999.
[6] R. Pöttgen, A. Fugmann, R.-D. Hoffmann, U.Ch. Rodewald, D. Niepmann, Z. Naturforsch. 55b (2000) 155.
[7] D. Niepmann, R. Pöttgen, B. Künnen, G. Kotzyba, J. Solid State Chem. 150 (2000) 134.
[8] Th. Fickenscher, U.Ch. Rodewald, D. Niepmann, R. Mishra, M. Eschen, R. Pöttgen, Z. Naturforsch. 60b (2005) 271.
[9] F. Stadler, Th. Fickenscher, R. Pöttgen, Z. Naturforsch. 56b (2001) 1241.
[10] S. Rayaprol, A. Doğan, R. Pöttgen, J. Phys.: Condens. Matter 18 (2006) 5473.
[11] R. Mishra, R. Pöttgen, R.-D. Hoffmann, D. Kaczorowski, H. Piotrowski, P. Mayer, C. Rosenhahn, B.D. Mosel, Z. Anorg. Allg. Chem. 627 (2001) 1283.
[12] S. Rayaprol, R. Pöttgen, Phys. Rev. B 72 (2005) 214435.
[13] S. Rayaprol, R. Pöttgen, Phys. Rev. B 73 (2006) 214403.
[14] A. Doğan, S. Rayaprol, R. Pöttgen, J. Phys.: Condens. Matter 19 (2007) 026209.
[15] R. Pöttgen, Th. Gulden, A. Simon, GIT Labor-Fachzeitschrift 43 (1999) 133.
[16] D. Kußmann, R.-D. Hoffmann, R. Pöttgen, Z. Anorg. Allg. Chem. 624 (1998) 1727.
[17] K. Yvon, W. Jeitschko, E. Parthé, J. Appl. Crystallogr. 10 (1977) 73.
[18] G.M. Sheldrick, Shelxl-97—Program for Crystal Structure Refinement, University of Göttingen, Germany, 1997.
[19] W.H. Zachariasen, Acta Crystallogr. 2 (1949) 94.
[20] K. Remschnig, T. Le Bihan, H. Noël, P. Rogl, J. Solid State Chem. 97 (1992) 391.
[21] J. Donohue, The Structures of the Elements, Wiley, New York, USA, 1974.
[22] R.-D. Hoffmann, A. Fugmann, U.Ch. Rodewald, R. Pöttgen, Z. Anorg. Allg. Chem. 626 (2000) 1733.
[23] R. Mishra, R.-D. Hoffmann, R. Pöttgen, Z. Naturforsch. 56b (2001) 239.
[24] I.R. Fisher, Z. Islam, P.C. Canfield, J. Magn. Magn. Mater. 202 (1999) 1.